Dynamics Model of a flexible Concrete Distributor Arm

Bulletin of Osaka Prefecture University
Series A, Vol. 46, No. 2, 1997, pp. 109−115

Dynamics Model of a Flexible Concrete Distributor Arm

Tatsuya NUNOHARA*, Kei SENDA**, Yoshisada MUROTSU**

(Received November 14, 1997)

This paper addresses the dynamics model of a flexible concrete distributor arm as long as 30 meters, which is articulated with 3 or 4 links. A linear mathematical model is derived by using a finite element method (FEM) model, a modal equation, and a modal damping. The obtained linear model is however inaccurate because the actual joint has a nonlinear resistance. For the controller design and analysis, the joint resistance is modeled by a standard joint resistance model with a Coulomb friction, an inertial resistance, and a viscous resistance. The modeling parameters are identified by the output error method, but the resulting model is not accurate enough. Finally, an acceleration dependent resistance model is constructed so as to represent a hysteresis loop appearing in resistance and joint velocity plane data of the vibration test. The derived model is adequate in terms of the agreement between the modeled resistance and the actually measured resistance.

1. Introduction

Concrete pump (C/P) vehicles in construction sites are indispensable to build reinforced concrete structures. The C/P vehicle has a distributor arm as long as 30 meters to deliver fresh concrete through a pipe along the arm. The arm with 3 or 4 links is articulated by rotary joints to adapt it to various construction sites as shown in Fig. 1. The arm has low stiffness because of the weight limitation, and its lowest natural frequency is 0.3∼0.5 Hz. Large vibrations are easily excited due to resonance because a pump pushes out the fresh concrete with pulsation whose frequency is close to the arm's natural frequency. The large vibration causes various problems and deteriorates the working condition, e.g., damage to the field under construction, danger to the worker controlling the delivery hosepipe, etc. Furthermore, the resonance causes large stress in the arm and the resultant fatigue shortens its life span. Therefore, it is important to suppress the vibration of the arm for the safety, the working efficiency, and the long life span.

The present authors have discussed on the vibration suppression using a hardware model simulating the real distributor arm.[1] In the study, the numerical simulations using a mathematical model were well agreed with the experimental results because the hardware model had small uncertainties. As mentioned later, the uncertainty in the real distributor arm cannot be ignored because the unmodeled dynamics, e.g., the friction in joints, affects control performance. The uncertainty in the mathematical model must be reduced for the controller design and analysis.

For the purpose, this study discusses the dynamics of the real distributor arm using some data of vibration excitation tests. A model well-agreed with the test data is finally derived after constructing a linear model using the finite element method (FEM), a standard joint resistance model, and a resistance model dependent on the joint acceleration.

2. Construction of C/P Vehicle and Vibration Test

2. 1 Construction of C/P vehicle

The C/P vehicle illustrated in Fig. 1 has the pump and the distributor arm for the fresh concrete delivery to the construction spot. The raw concrete of

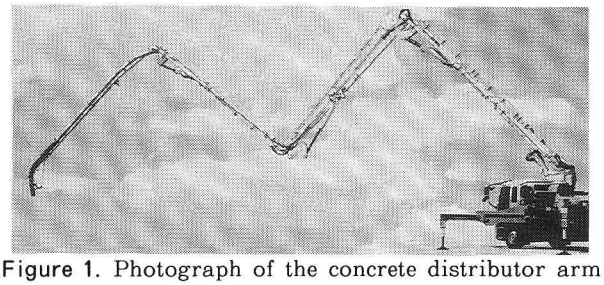

Figure 1. Photograph of the concrete distributor arm

* Graduate Student, College of Engineering
** Department of Aerospace Engineering

high viscous fluid is pushed out by the pump and transferred to the arm tip through a pipe along the arm. The distributor arm with 3 or 4 steel links is articulated by rotary joints to adapt it to various construction sites. Each joint has a joint drive cylinder powered by pressured oil, and the distributor arm can change its posture. The joints hold appropriate positions for a desired posture during operation by controlling oil flow in the joint drive cylinders. The distributor arm becomes structurally flexible because of the length of about 30 meters and the weight limitation. In addition, the joint drive cylinders have some compliance due to the compressibility of the oil. The lowest natural frequency of the arm is therefore as low as 0.3~0.5 Hz, which varies with posture change. Moreover, the pump pushes out fresh concrete with pulsation whose frequency is close to the arm's natural frequency. Hence, the large vibration is easily excited due to the resonance by the pulsation flow.

The first joint at the root has been reconstructed to control the joint drive force by adding control devices to the joint drive cylinder. Only the first joint has the control equipment because of the implementation restriction. Controllers are designed for this single input system to suppress the vibration. A schematic diagram of the control system is illustrated in Fig. 2. The control input is the oil pressure of the first joint drive cylinder. The pressure is controlled so that the bottom pressure, which is measured at the bottom of the joint drive cylinder, tracks the desired control input by a servo system using a vibration suppression cylinder. The joint angle cannot be measured directly but it can be calculated from the joint drive cylinder length, which is also calculated from the oil inflow volume measured by the position of the vibration suppression cylinder. The torque applied at the arm root is measured by a strain gauge put on the arm surface near the joint drive cylinder. The arm tip acceleration is measured with an accelerometer for vibration tests and control performance evaluations.

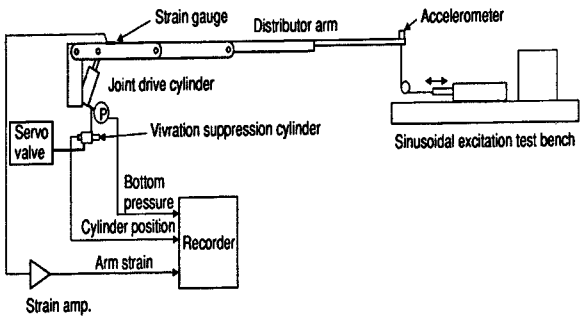

Figure 2. Schematic diagram of the control equipment and vibration test

2. 2 Vibration test

The distributor arm is excited by the applied force at the arm tip or a step-like motion of the second joint with a 465 kg tip mass. Sinusoidal loads are applied to the arm tip through a tension cable by the test bench. The amplitude of the sinusoidal loads is approximately 1,500 N. A preload of about 3,000 N is preliminarily applied because the cable transfers only a tension load. The obtained data during the vibration tests are the arm tip acceleration, the arm root torque measured with the strain gauge, the bottom pressure of the first joint drive cylinder, and the vibration suppression cylinder position.

3. FEM Model of Distributor Arm

A simplified model of Fig. 3 is considered for a mathematical model. Each link is described by a beam model with 2 finite elements. The articular joints connecting links are modeled as rotary springs, which represent the oil compressibility in the joint drive cylinders. The FEM model of the system can be obtained in the form

$$\boldsymbol{M}\ddot{\boldsymbol{x}}+\boldsymbol{D}\dot{\boldsymbol{x}}+\boldsymbol{K}\boldsymbol{x}=\boldsymbol{f} \tag{1}$$

where $\boldsymbol{M}$ is a mass matrix, $\boldsymbol{D}$ a damping matrix, $\boldsymbol{K}$ a stiffness matrix, $\boldsymbol{x}$ a state vector, and $\boldsymbol{f}$ a generalized force vector corresponding to $\boldsymbol{x}$. One obtains an MK-type eigenvalue problem by eliminating $\boldsymbol{D}$ in Eq.(1) where the i-th eigenvalue is λ_i and the eigenvectors compose a modal matrix $\boldsymbol{\Phi}$. By using the transformation

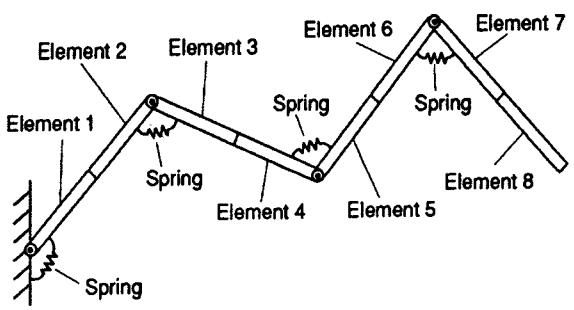

Figure 3. Finite element model of the arm

$$x = \Phi q \tag{2}$$

Eq.(1) is transformed into a modal equation

$$\ddot{q} + \Gamma \dot{q} + \Lambda q = \Phi^T f \tag{3}$$

where

Φ : M-normalized modal matrix satisfying $\Phi^T M \Phi = I$

$\Lambda \triangleq \Phi^T K \Phi = \mathrm{diag}[\lambda_1, \lambda_2, \ldots, \lambda_n]$

$\Gamma \triangleq \Phi^T D \Phi = \mathrm{diag}[2\zeta_1\omega_1, 2\zeta_2\omega_2, \ldots, 2\zeta_n\omega_n,]$

$\omega_i = \sqrt{\lambda_i}$: the i-th natural circular frequency

ζ_i : the i-th mode damping ratio

and a proportional damping for D is assumed.

The FEM model of Eq.(1) uses the designed parameters for links as well as the measured parameters of joint stiffness (1.57×10^8 N·m/rad) and modal damping ratios. The mathematical model and the FFT analysis of the vibration test response yield the direct accelerance from the excitation force to the acceleration at the arm tip as shown in Fig. 4. In this case, the arm stretches to its full length, i.e., all the links are horizontal, and all the joints are fixed by prohibiting oil flow in all the joint drive cylinders. The lowest four eigenmodes are used but the fifth and higher modes are ignored in the mathematical model for simplicity. The good agreement between the calculation and the measurement demonstrates the propriety of the mathematical model. The small error at the antiresonance is caused by the residual stiffness of the ignored higher modes. The obtained model is called a linear model in this paper.

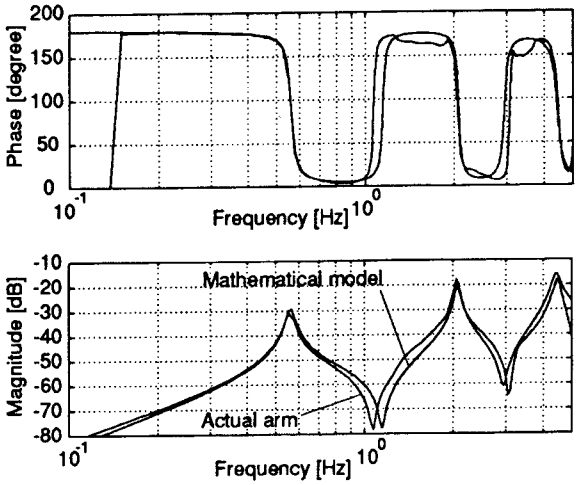

Figure 4. Direct accelerance at arm tip obtained from the actual arm and the linear mathematical model

4. DVDFB Control and Joint Friction

Direct output feedback controls are designed by using the mathematical model obtained in the previous section. To design the controllers, employed is the direct velocity and displacement feedback (DVDFB) control where the velocity and displacement sensor outputs are directly inputted into the collocated actuator. Its robust stability is well known and an appropriate choice of the feedback gains makes it an optimal regulator.[2] The control law employed here is

$$\tau_1 = -d\dot{\theta}_1 - \kappa \theta_1 \tag{4}$$

where

τ_1 : control torque to the first joint

θ_1 : angular displacement of the first joint

d, κ : positive gains of the velocity and displacement feedback

Figure 5 shows the direct accelerances at the arm tip computed from the obtained linear model for some feedback gains. The case 3 shows the best control performance among them.

Using those feedback gains, the DVDFB is exam-

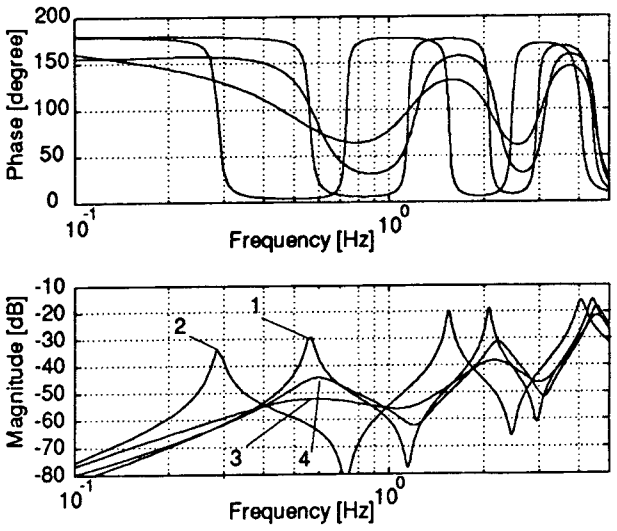

1 : $\kappa = 1.57 \times 10^8$ N·m/rad, $d = 0$

2 : $\kappa = 3.65 \times 10^6$ N·m/rad, $d = 0$

3 : $\kappa = 3.65 \times 10^6$ N·m/rad, $d = 3.65 \times 10^6$ N·m·s/rad

4 : $\kappa = 3.65 \times 10^6$ N·m/rad, $d = 1.00 \times 10^7$ N·m·s/rad

Figure 5. Direct accelerance at arm tip calculated by using the linear mathematical model controlled by DVDFB

ined for the actual distributor arm, but the control performance is not as good as the numerical results from the linear model. For example, the tip direct accelerances are compared in Fig. 6 between the actual arm and the linear mathematical model controlled by DVDFB of the following feedback gains:

$$\kappa = 3.65\times10^{6}\ \text{N·m/rad},\ d=0.0\ \text{N·m·s/rad} \quad (5)$$

There exists remarkable difference between the actual arm and the linear mathematical model, whereas no such differences are observed in Fig. 4.

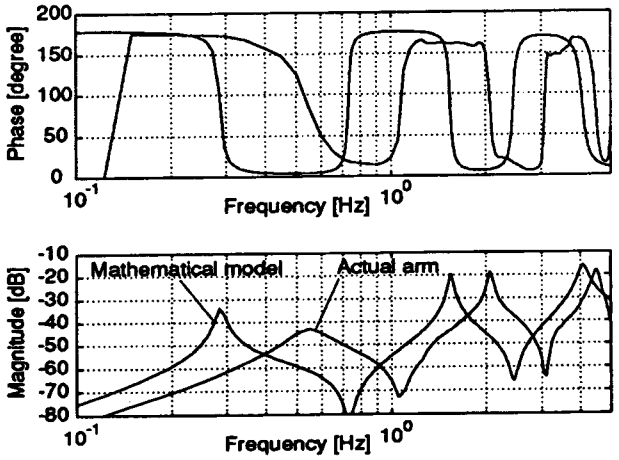

Figure 6. Direct accelerance at arm tip obtained from the actual arm and the linear mathematical model controlled by DVDFB

Some negative velocity feedback gains improve the control performance of the actual arm, while the same gains make the linear mathematical model unstable. The difference between the actual arm and the mathematical model is due to modeling errors, e.g., Coulomb friction, which are not considered in the mathematical model. In fact, Coulomb friction torque of about 30,000 N·m is observed in the first joint. A mathematical model comprised of the Coulomb friction yields the same phenomenon, i.e., the negative velocity feedback gains improve the control performance as occurred in the actual arm. For a controller design and analysis, it is now necessary to model and identify the joint resistance torque that is not considered in the previous linear model.

5. Modeling of Joint Resistance Torque

5. 1 Measurement of joint resistance torque

The data obtained during the vibration tests are the arm root strain measured with the strain gauge, the bottom pressure of the first joint drive cylinder, and the vibration suppression cylinder position. By using those measured variables, one can calculate the real torque τ_a applied to the arm, the joint drive torque τ_d generated by the joint drive cylinder, and the joint angle θ_1. The joint velocity $\dot{\theta}_1$ and the acceleration $\ddot{\theta}_1$ are derived from the angle θ_1. The joint resistance torque τ_f is given by

$$\tau_f = \tau_d - \tau_a \quad (6)$$

5. 2 Standard joint resistance model

The joint resistance torque can be modeled in the following form as generally used[3,4]:

$$\tau_f = C\,\text{sign}(\dot{\theta}_1) + I\ddot{\theta}_1 + D\dot{\theta}_1 \quad (7)$$

where the first term, the second, and the third in the right side denote the Coulomb friction, the inertial resistance, and the viscous resistance, respectively, and $\text{sign}(\dot{\theta}_1)$ is

$$\text{sign}\ (\dot{\theta}_1) = \begin{cases} 1 \text{ for } \dot{\theta}_1 > 0 \\ -1 \text{ for } \dot{\theta}_1 < 0 \end{cases} \quad (8)$$

This model is called a standard resistance model in this paper.

Figure 7 illustrates the time histories of the actual resistance torque τ_f and the modeled joint resistance torque $\hat{\tau}_f$ as the solid line and the broken line, respectively. The inputs are the step excitation and the sinusoidal excitations with 0.45 Hz, 0.55 Hz, and 0.7 Hz frequencies. The modeling parameters in Eq. (7) are estimated by the output error method, which minimizes the error e defined by

$$e = \left\{\int (\hat{\tau}_f - \tau_f)^2 dt\right\}^{1/2} \quad (9)$$

The following parameters are identified by using all the data of the step excitation and the sinusoidal excitations, i.e., the identified parameters are

$$C=1.1\times10^{3}\ \text{N·m},\ I=0.0\ \text{kg·m}^2,\ D=1.0\times10^{6}\ \text{N·m·s} \quad (10)$$

The identified model using the standard resistance model cannot achieve good agreement with all the actual responses as shown in Fig. 7. This discrepancy may result because the standard resistance model is

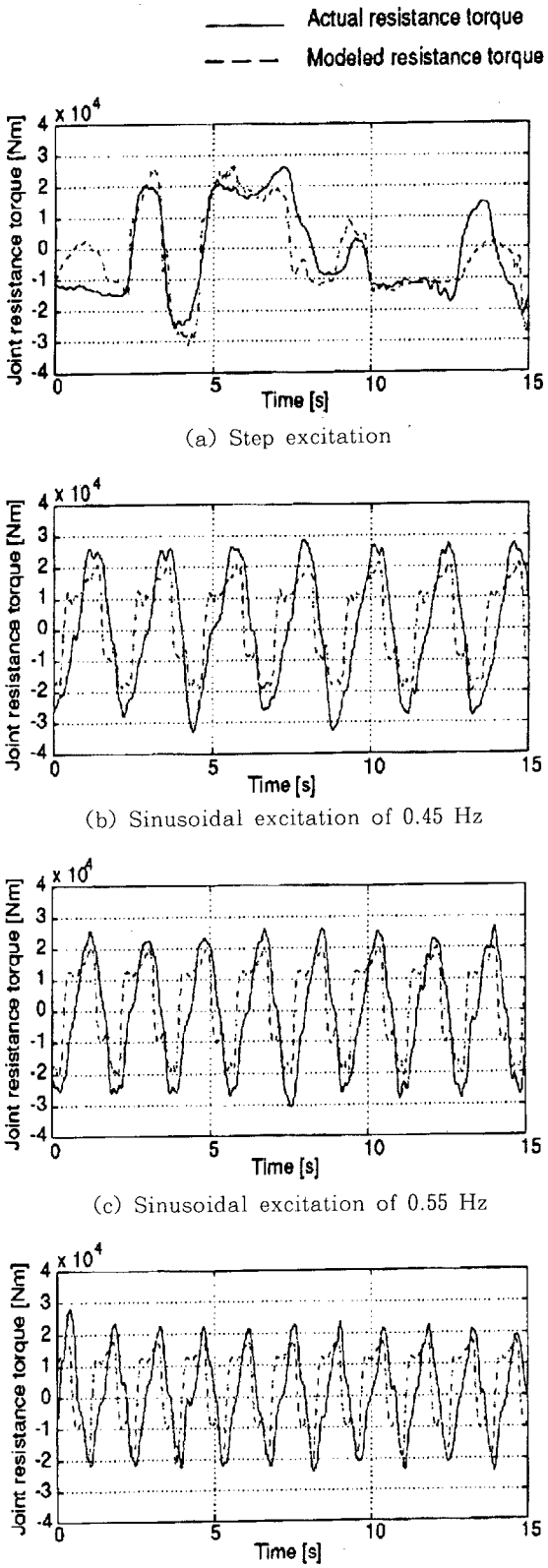

(a) Step excitation

(b) Sinusoidal excitation of 0.45 Hz

(c) Sinusoidal excitation of 0.55 Hz

(d) Sinusoidal excitation of 0.7 Hz

Figure 7. Time histories of torques at joint 1 obtained from the actual arm and the standard joint resistance model

not sufficient to describe the actual joint resistance.

5. 3 Acceleration dependent viscous resistance model

The solid lines in Fig. 8 show the responses for the step excitation and the sinusoidal excitations with 0.45Hz, 0.55Hz, and 0.7Hz frequencies, which are plotted on the plane of the joint velocity $\dot{\theta}_1$ and the joint resistance torque τ_f. A counterclockwise hysteresis loop is observed in all the cases. Therefore, the hysteresis loop is simply modeled as illustrated in Fig. 9 and divided into the following four phases

Phase 1 : OA ($\dot{\theta}_1>0$ and $\ddot{\theta}_1>0$)
Phase 2 : AE ($\dot{\theta}_1>0$ and $\ddot{\theta}_1<0$)
Phase 3 : OC ($\dot{\theta}_1<0$ and $\ddot{\theta}_1<0$)
Phase 4 : CF ($\dot{\theta}_1<0$ and $\ddot{\theta}_1>0$)

The joint resistance in each phase is modeled by the following viscous resistance

$$\hat{\tau}_f = D(\ddot{\theta}_1)\,\dot{\theta}_1 \tag{11}$$

where the viscous resistance coefficient D is a function of $\ddot{\theta}_1$. Figure 10 shows the graph of the viscous resistance coefficient $D(\ddot{\theta}_1)$ and the joint angular acceleration $\ddot{\theta}_1$ for the phase 1. A curve in the figure is the least square error curve, which fabulously represents the actual data. In the same manner, the viscous resistance coefficient curves are obtained for three other phases. The modeled resistance torque $\hat{\tau}_f$ computed by using this viscous resistance model is indicated by broken lines in Fig. 8. Figure 11 shows the numerical simulations using this acceleration dependent viscous resistance model under the same condition as that of Fig. 7. The acceleration dependent viscous resistance model is adequate because the modeled resistance $\hat{\tau}_f$ agrees well with the actual resistance τ_f.

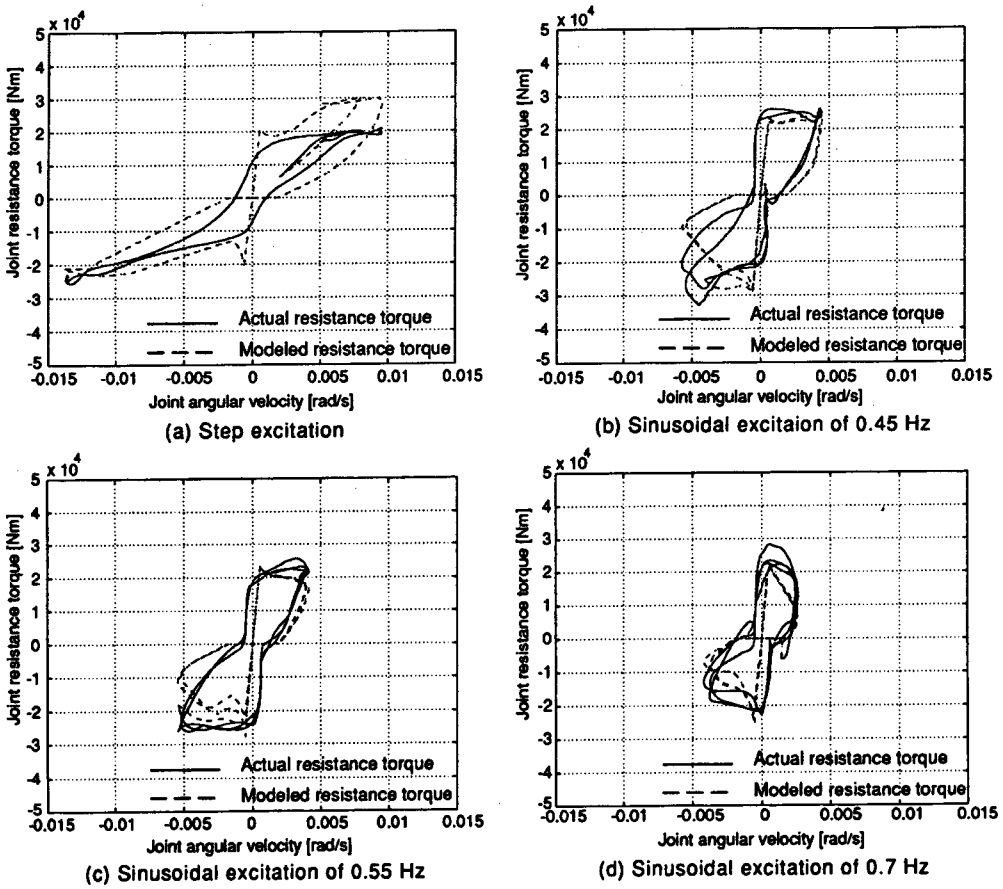

Figure 8. Graphs of the resistant torque and the velocity of joint 1

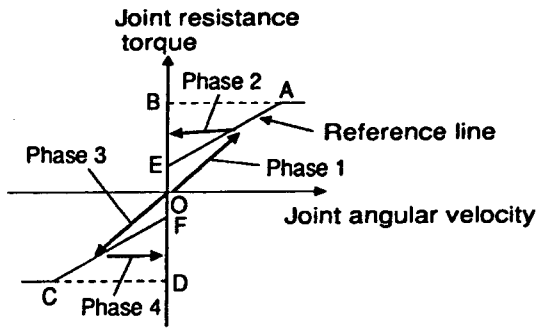

Figure 9. A hysteresis model of joint resistant torque

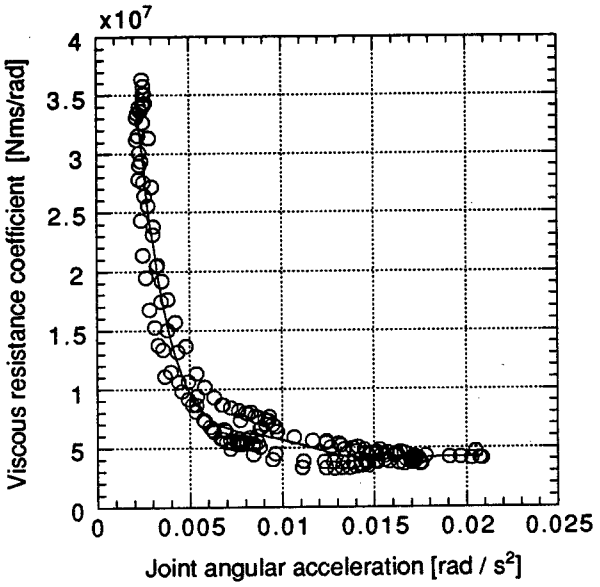

Figure 10 Viscous damping ratio as a function of the joint angular acceleration

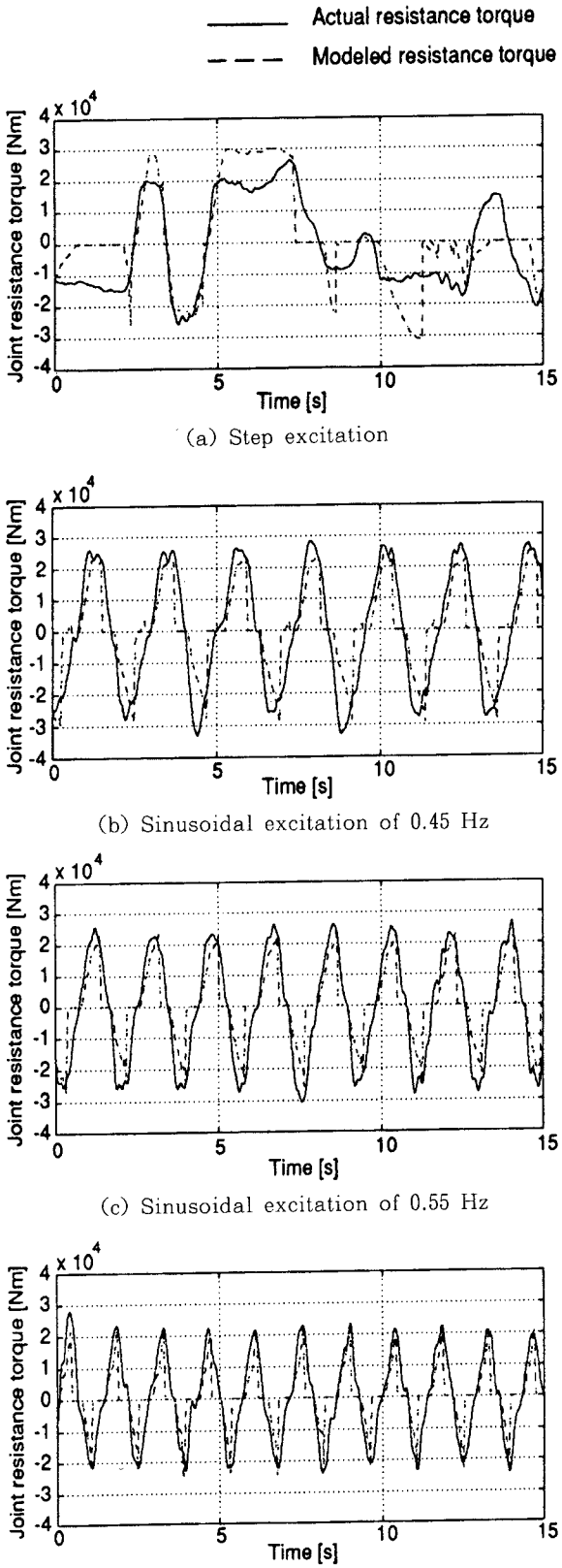

(a) Step excitation

(b) Sinusoidal excitation of 0.45 Hz

(c) Sinusoidal excitation of 0.55 Hz

(d) Sinusoidal excitation of 0.7 Hz

Figure 11. Time histories of torques at joint 1 obtained from the actual arm and the acceleration dependent viscous resistance model

6. Conclusion

This paper has discussed the dynamics model of the concrete distributor arm. The linear mathematical model has been derived by using the FEM model, the modal equation, and the modal damping. The obtained linear model has been inaccurate because the actual joint has the nonlinearity in resistance. For the controller design and analysis, the joint resistance has been modeled by the standard joint resistance model with the Coulomb friction, the inertial resistance, and the viscous resistance. The modeling parameters have been identified by the output error method, but the obtained model has not been accurate enough. Finally, the acceleration dependent resistance model has been constructed so as to represent the hysteresis loop on the resistance and joint velocity plane. The derived model has been adequate in terms of the agreement between the modeled resistance and the actually measured resistance. Physical meanings of the obtained model must be clarified in future studies.

References

1) Nunohara, T., Murotsu, Y., and Senda, K., "Vibration Suppression of a Flexible Concrete Distributor Arm (1st Report, Vibration Suppression Using DVFB)," Trans. Japan Society of Mechanical Engineers, Ser. C. (to appear in Japanese)

2) Koujitani, K., Ikeda, M., and Kida, T., "Optimal Control of Large Space Structures by Collocated Feedback," Trans. of Society of Instrument and Control Engineers, **25**(8), 882-888 (1989). (in Japanese)

3) Hirose, S., "Robotics－Vector Analysis of Mechanical System－," Shokabo, Tokyo(1987).(in Japanese)

4) Canudas de Wit, C., Noël, P., Aubin, A., and Brogliato, B., "Adaptive Friction Compensation in Robot Manipulators: Low Velocities," The International Journal of Robotics Research, **10**(3), 189-199 (1991).